Assessment of Spacecraft Operational Status Using Electro-Optical Predictive Techniques

Dave Swann and Bernie Klem
Aerospace Testing Alliance
Advanced Missile Signature Center
Arnold Engineering Development Center
Arnold AFB, TN
Brent McCoy
University of Oklahoma
Norman, OK

**For presentation at the
AMOS Technology Conference**

September 14 – 16, 2010

ABSTRACT

The current class of small satellite systems presents an analyst responsible for monitoring spacecraft operational status and early detection of detrimental anomalies with a broad variety of sensing and identification issues and challenges. Simple, small, cube-shaped satellites, without protruding solar panel appendages, may require enhanced preflight characterization processes to support monitoring by passive, remote, nonimaging optical sensors.

This paper will describe spacecraft optical signature modeling and simulation techniques to develop sensing and identification algorithms for observing and characterizing key spacecraft features. The simulation results are based on electro-optical signatures apparent to nonimaging sensors, along with related observable features derived from multicolor and multiviewing aspect scenarios. This model and simulation analysis capability is used to support programs to monitor spacecraft performance status and identify anomalies associated with spacecraft damage/deterioration due to space debris or micrometeorite impact, thruster exhaust deposition or material aging.

The development of state-of-the-art optical signature modeling tools to perform high-fidelity satellite models (such as the Air Force Academy FalconSat-5 or AFRL TacSat-3) simulations to characterize spectral radiant intensities apparent to passive, remote, nonresolved imaging sensors are described in detail. Simulations are performed for a comprehensive scenario range of natural (solar and earth) illumination and viewing conditions. Results are generated for comparing baseline, streamlined geometry models with the actual higher fidelity models that capture vehicle small-size hardware components and modifications.

Output consisting of radiant intensity history apparent to ground-based sensor locations for vehicle trajectories that capture a comprehensive range of illumination conditions from the sun and underlying earth scene are presented for extensive spectral band coverage spanning the electro-optical spectrum from visible wavelengths through extended long-wave infrared. The analysis of selected results is summarized with the perspective of developing future generation sensing and identification algorithms.

1. INTRODUCTION

Monitoring the operational status or health of spacecraft for early detection of detrimental anomalies presents a significant challenge to an organization or analyst responsible for the spacecraft. Critical components, such as solar panel arrays, sensors, and communication equipment, may require enhanced preflight characterization processes to support monitoring by passive, remote, nonimaging optical sensors.

While in orbit a spacecraft is exposed to a variety of hostile natural and man-made phenomena that can damage critical components on the spacecraft. Potential surface damaging events that can occur are (noncatastrophic) impact due to space debris or micrometeorites on surfaces of spacecraft that can affect the operational status of the system.

A more subtle surface modifying or damaging phenomenon is that due to exhaust plumes from thrusters on the spacecraft itself or nearby systems. In the low-atmospheric densities of space, thruster plumes can extend for thousands of kilometers. The damage to a spacecraft due to engine exhaust could result in a significant change in the optical properties of spacecraft solar panels and sensors.

When in orbit, spacecraft require onboard or secondary propulsion systems to perform orbit transfers, orbital maintenance, and attitude control maneuvers. A serious issue in the use of propulsion systems on spacecraft is plume impingement. In addition to generating unwanted torques and localized surface heating, impingement of a thruster plume on surfaces can produce surface contamination or degradation.

Thrusters are nominally positioned so that the exhaust plumes avoid potential impact on the surface structures of the spacecraft. However, under certain conditions the onrushing atmospheric wind of primarily O-atoms during certain Low Earth Orbit (LEO) maneuvers can deflect the exhaust plume to impinge on critical spacecraft components, such as solar panels or sensors. The potential contamination of spacecraft surfaces by engine exhaust plumes can degrade the performance of sensitive optical and thermal systems and affect mission performance.

The deposition of engine exhaust and plume contaminant material on sensitive spacecraft surfaces can modify the optical properties of the spacecraft surface materials, thus changing the absorptivity, emissivity, reflectivity, and transmissivity of certain functional spacecraft surfaces such as thermal control coatings, optical view ports and lenses, or solar panels. In addition to plume contaminant deposition on spacecraft surfaces, mechanical abrasion or surface material erosion resulting from exhaust-generated particulates (soot or ice particles due to condensation) can be swept back onto the spacecraft by the ambient atmospheric wind, essentially "sand-blasting" the spacecraft surfaces. Engine exhaust material deposited as plume contaminant layers on a surface could also produce surface chemical reactions, especially in the highly reactive O-atom surrounding atmosphere, and thus cause additional changes in surface properties.

The types of propellants used on the majority of spacecraft systems for orbital changes, attitude control, and other station keeping maneuvers include warm or cold gas monopropellants, pure hydrazine monopropellant thruster systems, and bipropellants using hydrazine derivatives such as MonoMethylHydrazine (MMH) and Unsymmetrical Dimethyl Hydrazine (UDMH).

The cold gas monopropellants typically used are H_2, N_2, NH_3, Freon, He, Ar, or Kr. These are primarily used on smaller spacecraft for attitude control and have typical thrust ranges of 0.05 to 200 N. These propellants can potentially produce condensed particles (droplets) in the exhaust, plus condensed (frozen) H_2O due to chemical interaction with the atomic oxygen in the atmosphere, which can be swept back onto the spacecraft surface by the ambient wind.

Pure hydrazine engine possible contaminants include water, unreacted hydrazine, NH_3, and ammonia hydrate. The specific engine parameters influence the amount of undecomposed hydrazine droplets which have been observed in both flight and ground tests to be significant in concentration. There have been successful measurements of detectable deposits from hydrazine rocket engine plumes in a high vacuum. Hydrazine is very reactive and can chemically react with surface materials to change optical properties. The water can freeze in the cold environment of space resulting in ice particles that can erode spacecraft surfaces if swept back onto the spacecraft.

For the MMH and UDMH propellants, significant amounts of H_2O, CO, and CO_2 exist in the exhaust plumes that can freeze in the space environment and potentially impact the spacecraft surfaces as condensed particles and change the optical properties of the surface materials. Carbon particles (soot) in the exhaust of these propellants can also be a potential source of contamination of spacecraft surfaces. Therefore, it is essential for operators of satellites and other spacecraft to be able to assess possible physical damage to their systems.

In this paper we explore possible means to assess spacecraft operational status and provide damage assessment using remote electro-optical measurements systems. The location of the sensor(s) to provide this assessment is not important, as either ground-based or space-based systems can be utilized. However, in the following analysis ground-based sensors are assumed. In either case, it is assumed the spacecraft observed by the sensor will be nonresolved, that is, it will appear as a point source to the detector.

2. METHOD

In this analysis we use computer models of a typical spacecraft to produce simulation hardbody signature data to determine whether ground sensors can detect changes to spacecraft surfaces due to plume impingement or space debris impact. These events can modify the optical properties of a surface material such as may be found on the solar panels. The goal is to develop a method for the prediction of contaminant effects on spacecraft surfaces using passive remote (nonimaging) sensors.

For this analysis, a satellite computer model similar to the TacSat-3 (Fig. 1) was constructed with arbitrary dimensions. The spacecraft dimensions were 1 m main diameter and 3 m total length. The three solar arms' dimensions were 0.57 m width by 2 m length. Ground-based sensors were chosen to perform detection in the 3.0 – 5.0, 8.0 – 12.0, and 14.0 – 21.0 μm spectral bands. These sensors were situated on Maui at the AMOS facility at an altitude of 3,048 m above sea level. The trajectory of the spacecraft was a fly-over of the AMOS facility with the atmospheric data recorded on 9 June 2009 starting at 0000 hr.
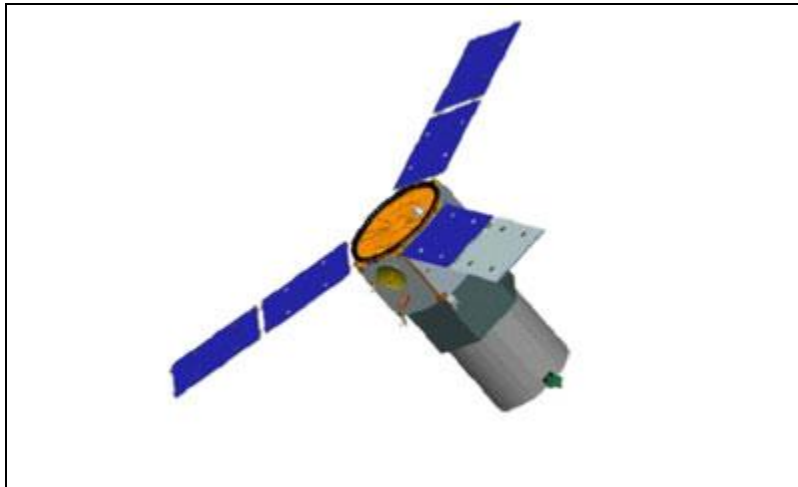

Fig. 1. Artist Conception of the TacSat-3 Satellite

To simulate degradation or soot deposition of the solar panels, selected areas of the solar arms were coated with black paint. The black paint optical and thermal properties are built into the signature generation program and were chosen because of the higher solar absorptivity and thermal emissivity relative to the other surface materials, as summarized in Table 1.

For the main body of the satellite model, varying aluminum alloys were used; the first hexagonal section and cylindrical section were composed of 2014-T4 aluminum, while the second hexagonal section was composed of an aluminum-zinc alloy. The solar arms were a base of the aluminum-zinc alloy overlaid with Silicon solar panel material. The connecting areas between each of the three sections were composed of silicon phenolic, and the band ring on the top of the satellite was chosen to be stainless steel. The antenna and other accessory components were composed simply of the aluminum-zinc alloy.

Figures 2 – 4 show three views of the TacSat-3 representative model used in the following analysis, given the dimensions and materials in Table 1.

Table 1. TacSat-3 Satellite Model Parameters

| Satellite Component	Material	Thickness (cm)	Thermal Emissivity	Solar Absorptivity
First Hexagonal Section	Aluminum (2014-T4)	0.75	0.1371	0.3986
Second Hexagonal Section	Aluminum Alloyed with Zinc (7075)	0.75	0.4002	0.1108
Cylindrical Section	Aluminum (2014-T4)	0.75	0.1371	0.3986
Caps for Hexagonal Sections	Silica Phenolic	0.5	0.5400	0.9085
Retaining Ring for Solar Panels	Stainless Steel	0.75	0.4124	0.1312
Solar Panels (Top)	Silicon Solar Cell	0.25	0.8044	0.7860
Solar Panels (Backing)	Aluminum Alloyed with Zinc (7075)	0.75	0.4002	0.1108
Added Instruments	Aluminum Alloyed with Zinc (7075)	0.75	0.4002	0.1108
"Damaged" Solar Panels	Black Paint of Lord Corp.	0.5	0.9500	0.8800
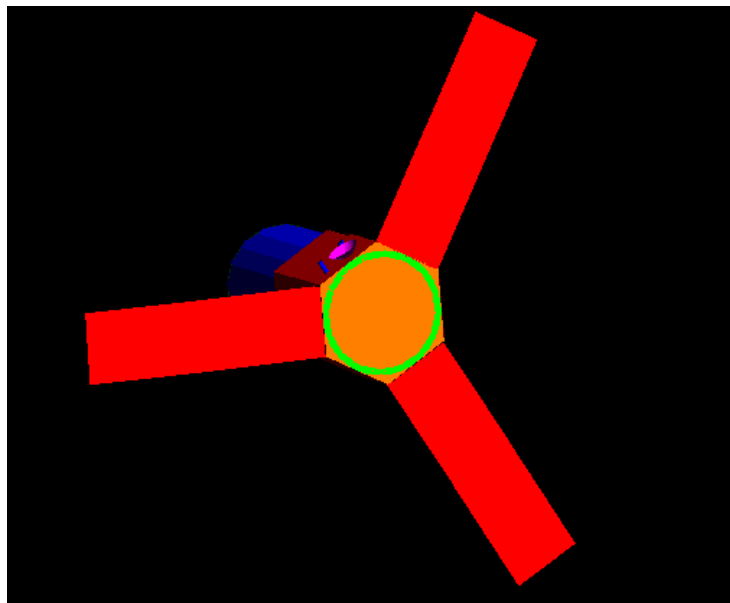
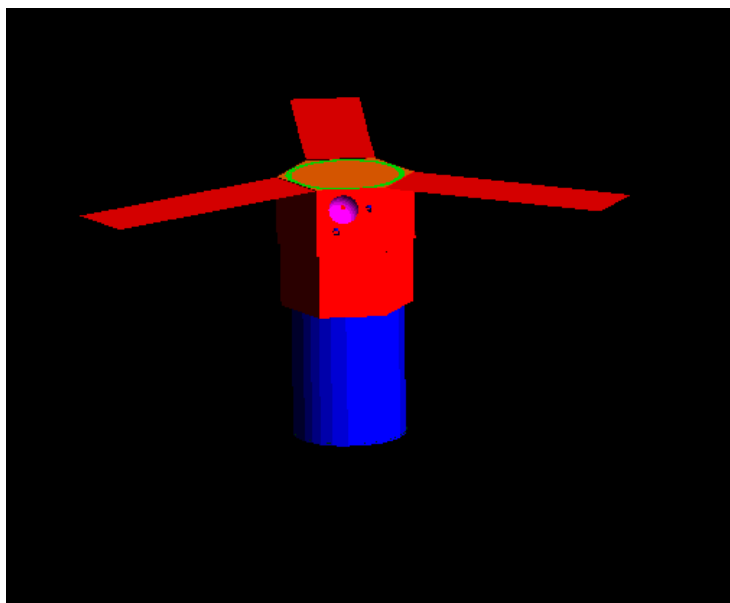Fig. 2. Top of TacSat-3 Satellite Model (Sensor Observation View)

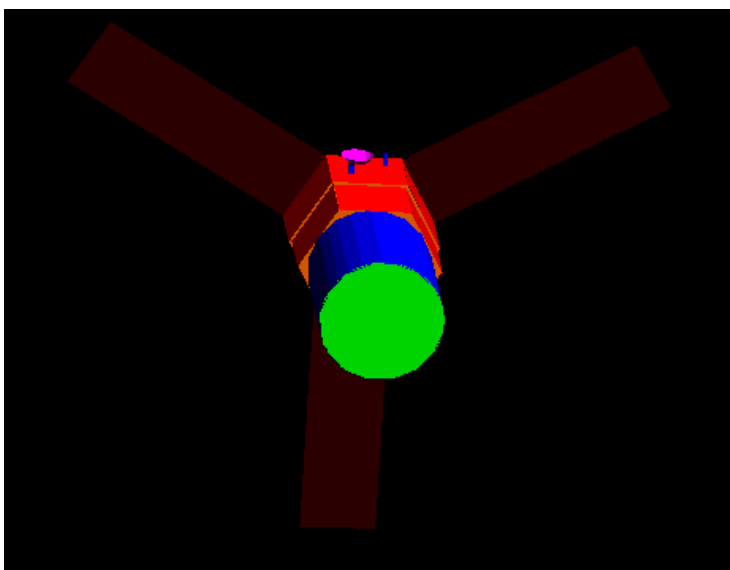Fig. 3. Side View of the TacSat-3 Satellite Model

Fig. 4. Bottom View of the TacSat-3 Satellite Model

To determine whether a change in the emissivity in a region on the solar panels (representing an area of plume contamination) is detectable from unresolved, radiometric signatures, several test cases were run with varying amounts of black paint cover on the three solar array arms on the satellite model. The amount of cover was systematically increased by the same increment each time by 0.1425 m^2 for each respective trial to simulate the detection of an observable pattern. Simulations were then performed to obtain the radiant intensities (J_1, J_2, J_3) for the 3 infrared spectral bands, (1) 3.0 – 5.0; (2) 8.0 – 12.0, and (3) 14.0 – 21.0 μm. From the radiant intensity simulation data, the corresponding three two-color temperatures (T_{12}, T_{13}, and T_{23}) and emissive areas (εA_{12}, εA_{13}, and εA_{23}) were determined.

The resulting color temperatures for six of the test runs are shown in Fig. 5. These represent no cover (baseline test), 0.2% cover (minimum detectable cover with size prediction error within 10%), 12.5%, 50%, and 100% (complete cover of all three solar panel arms). Note that although the change in the color temperatures in the 0.2% case is

virtually undetectable relative to the baseline case, the change in the values markedly changes (particularly the T_{23} color temperature) as the cover on the solar array panels is increased.
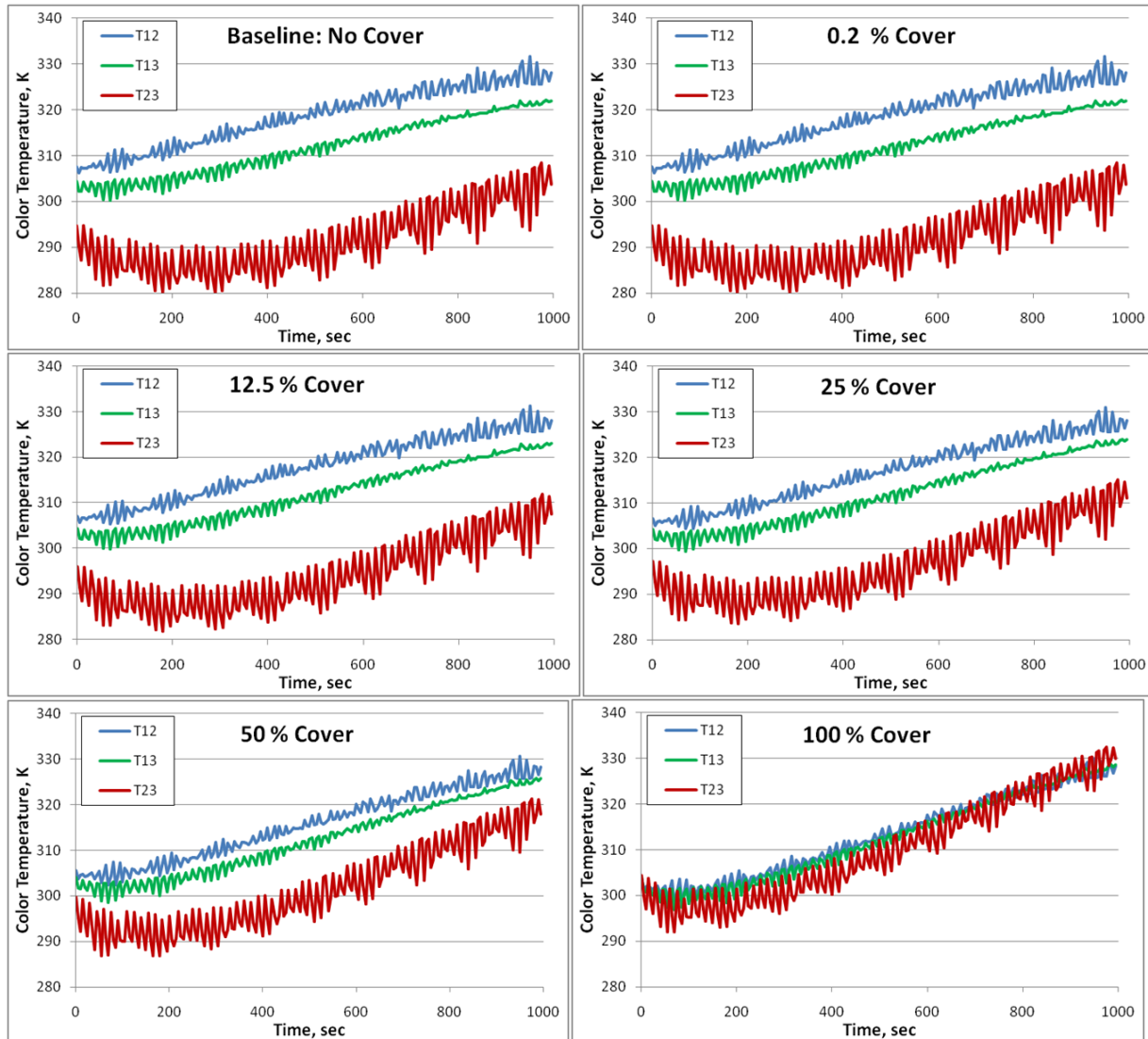

Fig. 5. Change in Color Temperatures as Contamination Cover on Solar Array is Increased

Using these results, the test cases were statistically evaluated to determine whether there was a noticeable, systematic change in the simulation data that could potentially correlate to the amount of cover on the panels. In this analysis, it was found that there was a strong linear correlation between the amount of black paint coverage on the solar arms and the signature detected by the ground sensors. A few preliminary regression fits to the simulation data were attempted, but these statistical analyses did not appear to be sufficiently robust or versatile. This was predominately due to the strict dependence that this type of analysis had on the conditions that were used for a particular test.

To provide a more robust statistical method of utilizing nonresolved signature data for damage assessment, a multiple regression approach was investigated. With this method, multiple data sets could be utilized simultaneously and referenced across their respective parameters collectively or independently. Other parameters could also be used, such as changing aspect angle and/or satellite motion (frequency oscillations due to rotation or spin), to more accurately determine the specific effects that certain physical aberrations, in this case solar panel corruption, can have on the target.

To incorporate the multiple regression approach, a MATLAB script was developed that accesses the data from individual CSV (comma separated variable) files containing the signature simulation data (spectral intensities, color temperatures, emissive areas, any other parameters) and stores the data in a structured array that can be easily accessed and utilized. These CSV files are created by extracting the required data from the optical signature generation code simulation output files. From that data, the code then computes the Multiple Linear Regression (MLR) analysis using the parameters specified from a list loaded into the collective structure of data.

Once the data are loaded and the "Calculate Coefficients" option is selected in MATLAB, the code accesses the specified data and performs the MLR. The MLR method is a way to solve the following equation:

$$T = X \cdot \beta$$

where T is an **n** x **1** vector containing the condition that is tested (in this case, the amount of cover on a solar panel), X is an **n** x **m** matrix containing data from the respective **n** simulation trials of each of the **m** parameters, and β is an **n** x **1** vector of coefficients that relates X to T and is the solution to the MLR. Since T and X are not necessarily square matrices, they may not have inverses that can be used to easily compute β.

To solve for β, the ML divide (\) operator in MATLAB is utilized ($\beta = X \setminus T$). If the normal equation is badly conditioned relative to the original system, the MATLAB ML divide operator avoids solving the matrices directly. Instead, to handle nonsquare matrices, a **QR** factorization orthogonal triangular decomposition method can be utilized in MATLAB to create a lower and upper triangular matrix from X and T whose product is evaluated numerically to produce an approximation of β. This process is quick and stable and produces a unique solution for β, but at the cost of adding some inherent error derived from both the approximations of the triangular matrices and the computation of their product. While this error is usually relatively small, on the order of 10^{-16}, it can potentially increase if X and T are not well conditioned. In this analysis, the simulation data (radiant intensity, color temperature, and emissive area) for the three bands (X) and solar panel contamination cover (T) are well-conditioned matrices. While this potential error is acknowledged, it is not directly calculated or incorporated into the analysis.

Table 2 shows an abbreviated (6 trial points) representation of the X matrix. Note that the X matrix (nominally 19 X 12, for all of the 19 trial points) as shown for this abbreviated case is a 6 x 12 array so that the two separate tables (shown in Table 2 as 6 X 6 arrays stacked on top of each other for convenience of presentation) are actually oriented side by side. In addition to the nine optical parameters (three intensities, three color temperatures, and three emissive areas) provided by the simulation code, an AC (alternating component) parameter was added to the matrix that accounts for anomalies in the motion (rotation, spin) of the spacecraft. The AC component is determined using a wave packet analysis approach by computing the Fourier Transform of each radiant intensity band for a specific trial, multiplying it by its complex conjugate, and dividing it by the total time-span of the data. To convert this into a single fractional value corresponding to each band, the resulting data are summed over a user-selected range or as a default from the fifth data marker on, and the result is normalized with respect to the initial, or peak, value obtained from the transform. The use of this component allows the MLR analysis to avoid any sharp peaks caused by anomalies (such as solar glint) in the periodic rotational satellite motion that appears in the simulations as a response to the observation of the covered areas on the solar panels.

Table 2. A Selection of the First Six Entries in the *X* Matrix (Shown Stacked for Convenience)

Color Temperature Bands 1-2	Color Temperature Bands 1-3	Color Temperature Bands 2-3	Emissive Area Bands 1-2	Emissive Area Bands 1-3	Emissive Area Bands 2-3
318.491	311.657	291.615	2.443	3.056	3.737
318.472	311.652	291.650	2.444	3.056	3.735
318.459	311.655	291.693	2.446	3.056	3.735
318.434	311.657	291.768	2.449	3.058	3.733
318.385	311.668	291.943	2.456	3.060	3.730
318.331	311.679	292.127	2.463	3.063	3.727
Radiant Intensity Band 1	**Radiant Intensity Band 2**	**Radiant Intensity Band 3**	**Fractional AC Band 1**	**Fractional AC Band 2**	**Fractional AC Band 3**
8.663	124.904	122.864	2.91E-05	9.54E-06	3.12E-06
8.662	124.918	122.849	2.90E-05	9.48E-06	3.09E-06
8.665	124.989	122.884	2.90E-05	9.48E-06	3.09E-06
8.669	125.099	122.930	2.91E-05	9.50E-06	3.10E-06
8.682	125.370	123.051	2.94E-05	9.59E-06	3.13E-06
8.695	125.656	123.180	3.00E-05	9.77E-06	3.21E-06

Table 3 gives the values in the *T* matrix or the different solar panel coverage test cases. The areas here correspond row by row to the data in matrix *X*.

Table 3. T Matrix, Representing the Different Solar Panel Coverage Test Cases

Test Cases (m^2)
0
0.007
0.014
0.0285
0.057
0.0855
0.1425
0.285
0.4275
0.57
0.7125
0.855
0.9975
1.14
1.71
1.71
2.28
2.85
3.42

As can be seen from Table 2, elements of matrix *X* are singular values. This is a necessary restriction on *X* due to the nature of the computation. For that reason means are used for each data type and sensor combination. Therefore, the means of the radiant intensities and color temperatures used for each of the three bands were used in the analysis.

3. ANALYSIS RESULTS

The MLR method allows an analyst to access several parameters simultaneously and, unlike principal component analysis, utilize them collectively to determine how a certain parameter affects the simulated data (i.e., how solar panel aberration affects the radiative signature). It is also a robust and versatile method since it is generically conditioned according to changes defined in the model and the parameters that are used to describe those changes. The computations, time-wise, are relatively fast using current computer systems, and the methods used within the computation are stable, which prevents errors that could potentially arise from small input changes.

The primary parameter investigated in the development of this method was the amount of solar panel area (m^2) covered by black paint. This was an arbitrarily chosen parameter and could easily be changed to another metric, such as the addition of various size features on the spacecraft at a given location, if desired. Also, for this preliminary analysis, we chose to use only the radiant intensity, color temperature, and emissive area simulation measurement data for our calculation of β in order to obtain the most accurate information possible. Other possible parameters that could be used in the analysis would be sensor-target observation angle or range. In the trajectory and observation geometry investigated in this analysis these parameters were not an issue. In other observation geometries, corrections due to these factors would be necessary.

The Multiple Linear Regression analysis predictions of the solar panel area coverage, compared with the actual coverage used for the nonresolved signature simulations, are given in Table 4. The 0 m^2 trial (no solar panel coverage) provides an estimate of the inherent error (0.067%) of the MLR method. A plot of these results, comparing the predicted solar panel coverage with the actual values used in the simulations, is shown in Fig. 6.

Table 4. Multiple Linear Regression Analysis Predictions vs. Actual Coverage

| Trial Number	Actual Amount of Cover (m^2)	Predicted Amount of Cover (m^2)	Percent Error (%)
1	0	-0.0007	0.0668
2	0.007	0.0075	7.3971
3	0.014	0.0148	5.3647
4	0.0285	0.0282	1.1770
5	0.057	0.0562	1.4836
6	0.0855	0.0854	0.1220
7	0.1425	0.1429	0.2755
8	0.285	0.2856	0.2007
9	0.4275	0.4272	0.0784
10	0.57	0.5707	0.1200
11	0.7125	0.7123	0.0315
12	0.855	0.8551	0.0115
13	0.9975	0.9970	0.0496
14	1.14	1.1396	0.0364
15	1.425	1.4264	0.0994
16	1.71	1.7103	0.0190
17	1.71	1.7100	0.0012
18	2.28	2.2805	0.0214
19	2.85	2.8495	0.0191
20	3.42	3.4202	0.0046
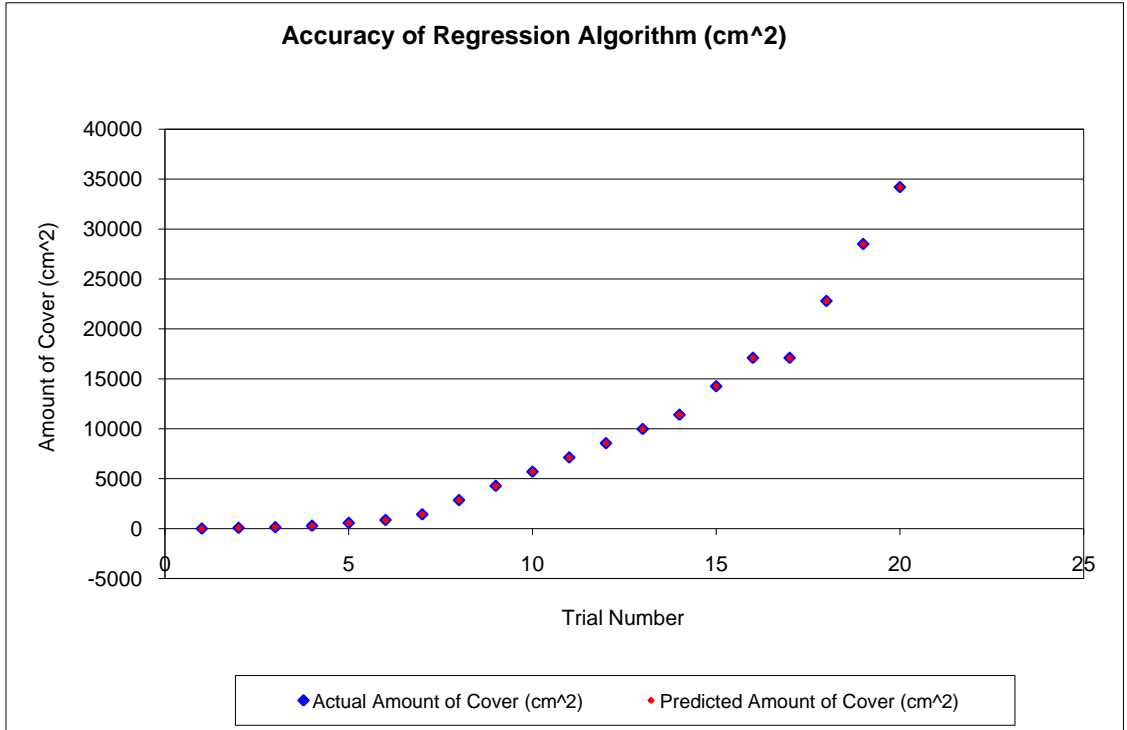
Fig. 6. Predicted vs. Actual Solar Panel Coverage

As we can see, the algorithm is capable of predicting the amount of cover on a solar panel with reasonable accuracy for smaller spot sizes and excellent accuracy for larger values. For example, trial #20 is the best case scenario for solar panel corruption detection and quantification, representing the case where all 3 solar panels (total area 3.42 m^2) are covered with the black paint. On the other hand, trial #2, with surface area coverage of 7 X 10^{-5} m^2, represents an extremely small feature (0.205% of the entire solar panel area or 0.614% of one solar panel), yet the MLR analysis estimates the size from the nonresolved signatures to within 7% accuracy.

The results of this analysis also show (see Fig. 7) that as the area coverage decreases from 500 down to 70 cm^2, there is a rapid increase in the error associated with the MLR prediction, so that for areas less than 70 cm^2 the experimental error would be greater than 10%, which is the minimum requirement for acceptable estimates. It should be noted that these results will be specific for the current configuration and simulation parameters. The results could be much different for other trajectories, illumination conditions, sensor bands, or spacecraft configurations. This algorithm needs to be (and will be) tested for other spacecraft configurations and variations in the simulation parameters.
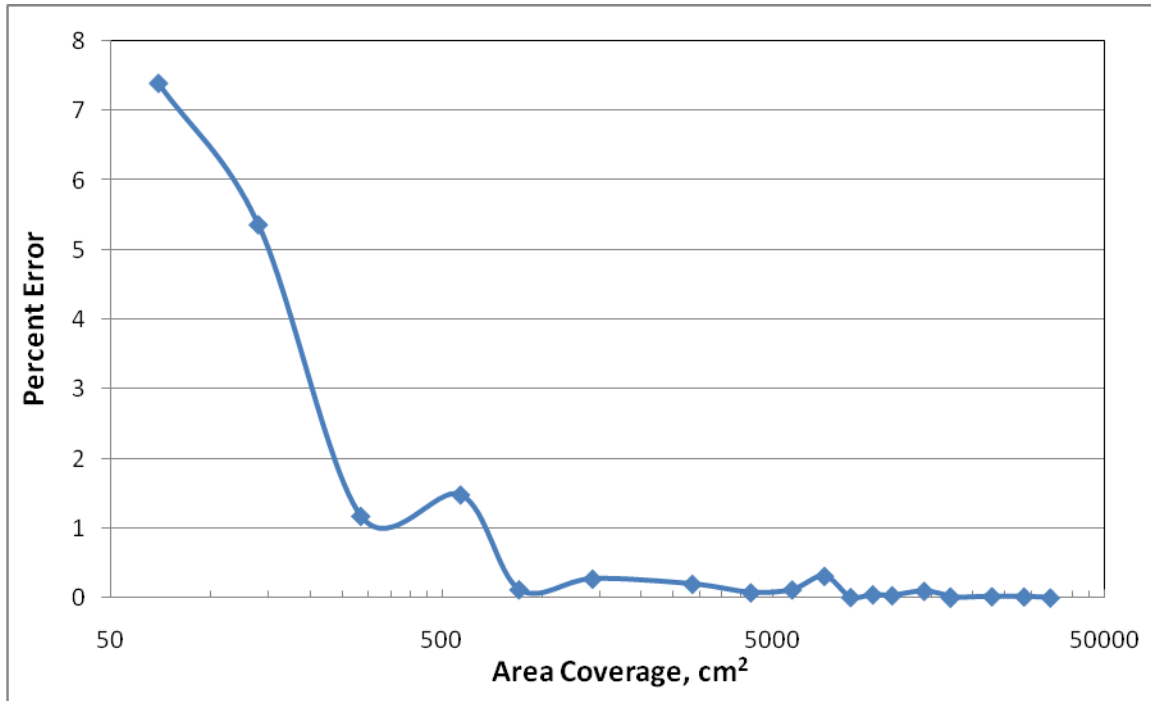
Fig. 7. MLR Estimation Error vs. Actual Area Coverage

4.   DISCUSSION/FUTURE STUDY

This analysis should be viewed only as a proof of concept in the sense that the correlation and algorithm developed is not necessarily a solution to fit all circumstances and would need additional analysis, test, and evaluation in order to be completely general and valid for all potential sensing and identification scenarios. The analysis presented in this paper is a first step in the generation of a method for providing surface area coverage predictions.

In a real-time mode one would want to solve the two trial cases (no coverage representing the baseline measurement and an unknown partial coverage) using the parameters (radiant intensity, color temperature, emissivity area) for multiple observation times to increase the statistics.

Once fully developed, however, this technique could have potential application in any health monitoring situation where the anomaly of interest can be observed by passive remote sensors. A necessary requirement is that the anomaly on the spacecraft must have identifiable thermal and/or optical (emissive, reflective) characteristics that will produce a measureable change in the observed unresolved spectral signature. In this regard, more study is required on how different material compositions can affect the detectability of solar panel aberrations.

Developing a generalized algorithm will focus on improving the validity of the correlations to make it more applicable to all cases of interest. In addition to using the Multiple Regression Technique to characterize all detectable aberrations or anomalies, a single-correlation vector technique could also be applied to such phenomena to provide sufficiently accurate predictions.

This approach that was developed for use in detecting and analyzing the condition of the solar panels could be used to evaluate changes in other regions of spacecraft, such as the addition or deployment of antennas and other hardware features. This would enable personnel utilizing the spacecraft to be able to determine or confirm from remote ground optical sensors that experimental packages or solar panels have properly deployed.

Future investigations will evaluate how viewing angle and trajectory affect the prediction capabilities of the correlation, i.e., how much better the matrix β can identify and predict the size of anomalies on spacecraft for more complex trajectories than the Maui fly-over used in this analysis. Trajectory dependent parameters will be required

to improve the accuracy, increase the usability, and make the algorithm more general. In this regard, we propose using sensor observation, or aspect angle and range corrections, to source correct the data.

As noted in this paper, the particular development of the correlation vector, $\boldsymbol{\beta}$, did not address or include the errors associated with the numerical approximations. It is possible to include an error term, $\boldsymbol{\varepsilon}$, in the MLR method format that may further improve the accuracy of our algorithm. In this case we have the expression,

$$T = X \cdot \boldsymbol{\beta} \pm \boldsymbol{\varepsilon}$$

In this equation, $\boldsymbol{T}$, $\boldsymbol{X}$, and $\boldsymbol{\beta}$ are as before and $\boldsymbol{\varepsilon}$ would be a matrix or vector containing the errors associated with the computation of $\boldsymbol{\beta}$. In general, $\boldsymbol{\varepsilon}$ can be positive or negative. For our correlation, however, we would require that $\boldsymbol{\varepsilon}$ be negative in order to minimize errors due to the numerical approximations. The investigation and possible inclusion of the error associated with this process could improve the prediction algorithm for remote detection and characterization of spacecraft anomalies.

Additional investigation is required to determine how detailed the characterization of a particular phenomenon needs to be to develop an accurate algorithm. In the current analysis we achieved acceptable accuracy, approximately 90%, with 12 parameters and 19 different characterizations of those parameters, i.e., 19 different trials with varying amounts of solar panel cover in each trial. It would be of significant interest to investigate how few parameters and characterizations could have been used to achieve similar accuracy.